Investigations into the Tectonic Faults on Magadi Geothermal Field Using Ground and Aeromagnetic Data

A. A. Komolafe[1,*], Z. N. Kuria[2], T. Woldai[3], M. Noomen[3], A. Y. B. Anifowose[1]

[1]Department of Remote Sensing and Geoscience Information System, Federal University of Technology, Akure, Nigeria

[2]Department of Geology, University of Nairobi, Kenya

[3]University of Twente, ITC, Enschede, Netherlands

.

ABSTRACT

Lake Magadi area of the Kenya Rift is characterized by faulting, tectonic activities and geothermal resources. The geothermal potential of the graben in the southern part of the lake was investigated using magnetic methods (ground and airborne). This was done to determine the geometry of tectonic faults and ascertain their influence on the flow of hot springs, which are manifested on the surface. Five N-S faults were identified for ground investigation using ground magnetic survey. Magnetic data were processed using vertical derivatives, analytical signal and Euler deconvolution. The faults were further mapped with aeromagnetic data using 2D Euler deconvolution. Magnetic derivative grids and profiles revealed subsurface faulting/tectonic activities up to a depth of 400m and the presence of fluid-filled zones within the basin, which are marked by the absence of magnetic sources. A deeper investigation into the lineaments from the aeromagnetic data showed that the surface faults extend into a depth of 7.5 km in the subsurface. The alignment of magnetic sources at the rift axis showed that these faults are probably the parallel faults which bound the basin/graben to the west and to the east. The N-S faults structures in the south of the lake serve as conduits for fluids which support the upward flow of the hydrothermal fluid along its margin.

1. INTRODUCTION

The roles of faults and fractures on crustal fluids have been of major interest in earth sciences, including geology, seismology, hydrogeology and petroleum geology [2]. The static and dynamic effects of different stresses on rocks often produce change in rock mass such as fractures, faults and in general permeability which in turn control the flow of fluids in the earth crust. [3] define fractures and faults are planes of tensile or shear failure at microscopic to regional scales in brittle rocks. These faults and fractures are developed mostly in competent rocks within the earth crust. In case of fractures, they are usually developed when the stress applied exceeds the elastic limit of the rock [3]. These two deformations are of great importance in crustal fluid distributions and control. The movement of crustal fluids (in this case, hydrothermal) to the surface from the reservoir rock depends of the pressure, temperature and most importantly the presence of active faults and fractures in the subsurface which are extended to the surface.

* Tel.: +2348037899856.
E-mail address: aakomolafe@futa.edu.ng

.

Geothermal resources, according to [4] are generally associated with tectonically active region which are generated as a result of temperature differences between the different parts of the asthenosphere (below the lithosphere) where convective movement are formed. This slow convective movement is said to be maintained by the radioactive elements and heat from the deepest part of the earth. The less dense deep hotter rocks tends to rise with the movement towards the surface while the colder but heavier rocks close to the surface tend to sink, re-heat and rise again. Generally, geothermal system is made up of the heat source, the reservoir, the recharge area and the connecting paths such as faults and fractures through which fluids percolates to the reservoir (the host rock) and in most cases are escaped to the surface as fumaroles and hot springs. The heat source is often assumed to be magmatic intrusion that has reached shallow depths (5-10km) [4]. The reservoir rocks are permeable rocks through which fluids circulates and extracts heat from the heat source. This is overlain by impermeable rocks and is connected to a surficial recharge area. Through fractures, meteoric water replaces or partly replaces the fluids which escape from the reservoirs as springs or during drilling.

Geothermal activities are associated with most parts of the Kenyan rift valley. The warm and hot springs are mostly connected to the lakes through various conduits [5]. Geothermal manifestations have been indentified at different locations in the study area (Figure 1), the most active and currently producing being the Olkaria geothermal field the northern part [1]. It exists within an old caldera complex, with surface manifestations in form of hot springs. It is associated with N-S normal faulting as observed by [1] in the southern part of the rift (Magadi). Lake Magadi water is mostly derived from underground hot water inflow with a continuous recharge from the surface waters [5-6]. Unlike some other geothermal regions where the reservoirs containing hot fluids have to be penetrated during exploitation, geothermal resources around Lake Magadi are clearly manifested on the surface in the form of hot springs and trona deposit along the lake margin and in the lake respectively. These surface manifestations of the hot springs have been attributed to continuous tectonic activities and the presence of various faulting systems in the area [6-7]. The role of N-S faults in the south of Lake Magadi as major conduits for geothermal resources and the deposition of trona in the lake have been proposed by [6] but not yet investigated, hence the focus of this study in order to know the flow paths of hydrothermal fluids with the aim of understanding the geothermal potentials.

[8] Investigated the proposed influence of the tectonic faults at Lake Magadi using geoelectric method. Their investigations revealed an upward flow of saline hot water to the surface via the fault splay; this was revealed by the relatively low resistivity within the profile. To further probe the claim, ground magnetic method with constraint from the airborne magnetic was applied to investigate the geometry of the N-S faults in the south of Lake Magadi and determine their influence on the expression of geothermal resources such as hot springs and trona deposits.

Magnetics method is very effective in studying structures and delineating depth to heat source in geothermal environments [8-10]. This study employs the use of magnetic methods (ground and airborne) to investigate the geometry of the N-S faults in the south of Lake Magadi and determine their influence on the expression of geothermal resources such as hot springs and trona deposits.
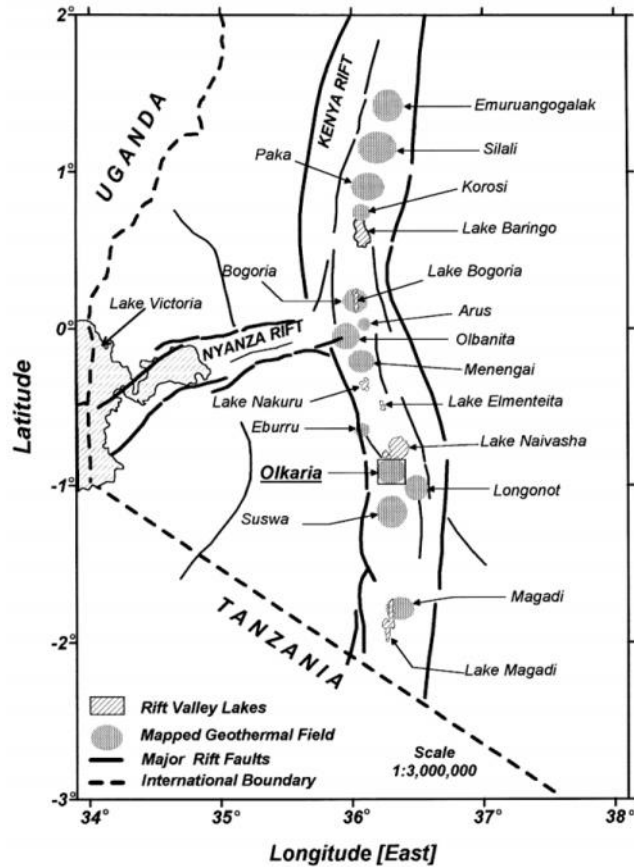
* Tel.: +2348037899856.
E-mail address: aakomolafe@futa.edu.ng
.

73

Figure1: Location of significant geothermal areas in the Kenya Rift
Valley (Source: [1]).

1.2. THE STUDY AREA

Lake Magadi area is the southernmost part of Kenya Rift, 120km southwest of Nairobi and 20km north of the Tanzanian border. It is located within Latitudes 1°40'S and 2°10'S, and Longitudes 36°00'E and 36°30'E, characterized by a flat rift floor [11] (Figure 2). The approximately 100km^2 size lake is recharged by saline hot springs (between 26°C and 86°C) along the lake margins [6]. Most of the hot springs lie along the north-western and southern shorelines of the lake. The lake comprises of trona deposit ($Na_2CO_3.NaHCO_3.2H_2O$) about 40m thick, covering about 75km^2 resulting from the concentration of different water sources, especially hydrothermal fluid [6]. According to [12] after a chemical analysis of collected waters, Magadi trona results from the evaporated concentration and mixing of waters from three sources namely dilute surface inflow, relatively deep hot and concentrated groundwater reservoir, and cold concentrated surface brine. An analysis of the water revealed five distinct hydrologic stages in the evolution of the water compositions viz: i) the dilute stream flow, ii) dilute ground water, iii) saline ground water (or hot springs reservoir), iv) saturated brines, and v) residual brines [6]. The active alkaline volcanoes in the area through hydrothermal systems circulation supply the saline (alkaline brine) hot springs. For the purpose of this study, sampling points located close to the hot springs in the southern part of the Lake were selected (Figure 2).

* Tel.: +2348037899856.
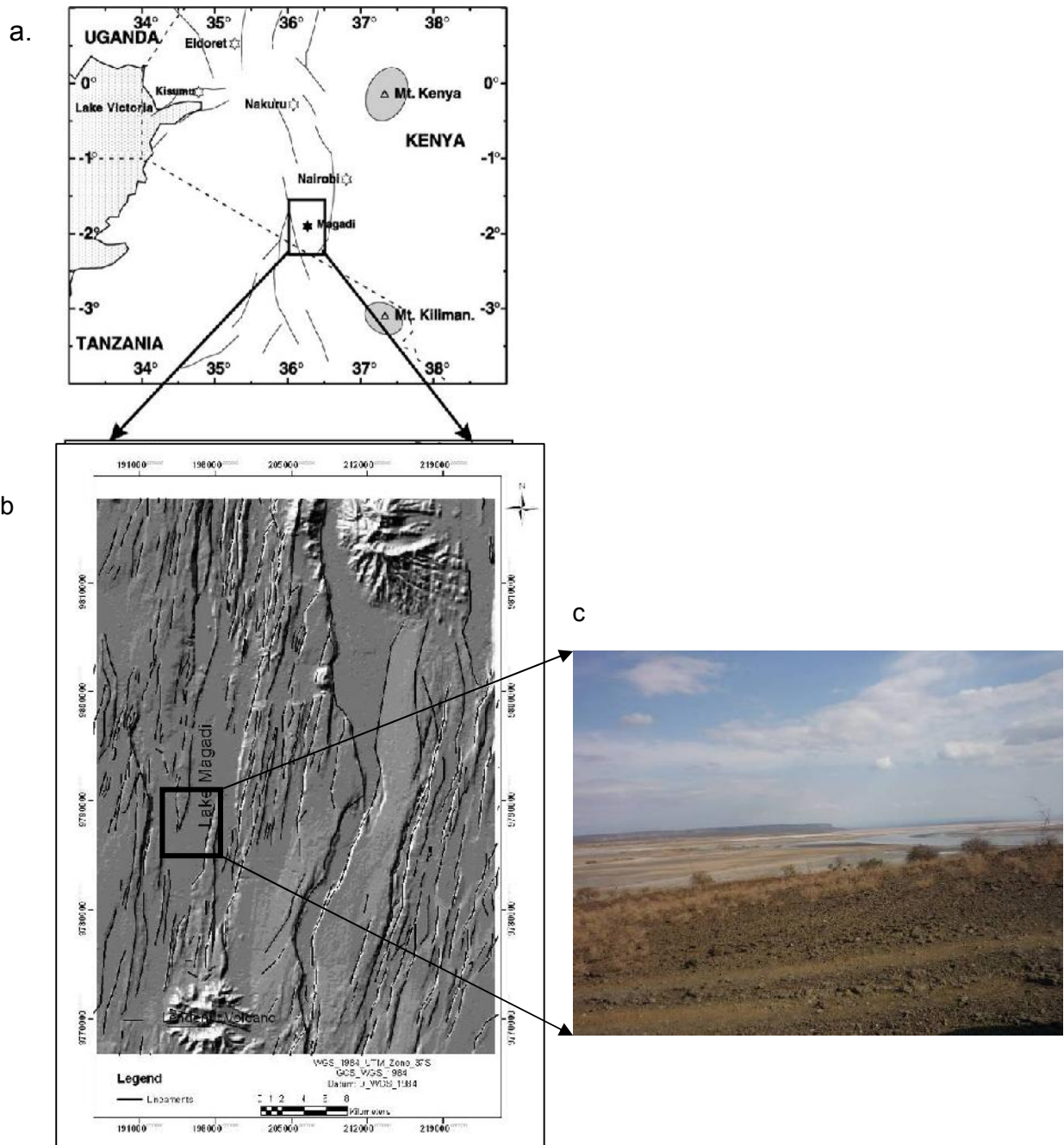E-mail address: aakomolafe@futa.edu.ng

.

Figure 2 (a) Geographic location of Magadi area (Adapted from [11], (b) Lineament map of Lake Magadi overlain on SRTM DEM **(c)** The study area and associated springs**.**

GEOLOGY OF LAKE MAGADI

[13] described the geology of Lake Magadi as being made up of mostly Archean to early Paleozoic crystalline basement rocks and rift-related volcanics and sediments (Figure 3). The rock succession can be grouped into Precambrian metamorphic rocks, Plio-to Pleistocene volcanic rocks, and Holocene to Recent lake and fluvial sediments [11]. The oldest rocks in the area are the quartzites, gneisses and schists of Archean age. The extrusion of alkali trachytes within the lake as explained by [14] and [15] occurred in the Pleistocene age. In the southern and northern ends of the Lake Magadi area, there is a deposition of irregular interbedded chert rocks which consists of silicified bedded clays on top of alkali

* Tel.: +2348037899856.
E-mail address: aakomolafe@futa.edu.ng
.

152 trachytes [11, 16]. This is unconformably overlain by a thin layer of lake beds known as the Oloronga
153 beds, followed by a series of sub-parallel faulting system that resulted in the formation of the Lake Magadi
154 rift floor. The formation of the Quaternary sediments exists within a fault-bounded basin.
155 An integrated seismic, drill hole data and gravity model by [17] revealed sediments and volcanic complex
156 at the rift floor adjacent to Nguruman escarpment. Their model explained the crustal structure of Lake
157 Magadi as having basement rocks at the bottom which are exposed at the western (Tanzanian craton)
158 and eastern (Mozambique belt) flanks, and overlain by Pliocene to Miocene volcanic and sedimentary
159 rocks. The Rift has been discovered to exist in the boundary between the Archean Tanzanian craton and
160 Neoproterozoic Mozambique belt, which is characterized by a complex fault zone [13]. The tectonic
161 settings and structures of Lake Magadi are influenced by three factors, namely stable Tanzanian Craton,
162 Aswa shear zones, and southern fringes of the Kenya dome [18]. The four major fault sets associated
163 with the Kenya rift (normal N-S fault, dextral NW-SE fault, strike slip ENE-WSW fault and sinistral NE-SW
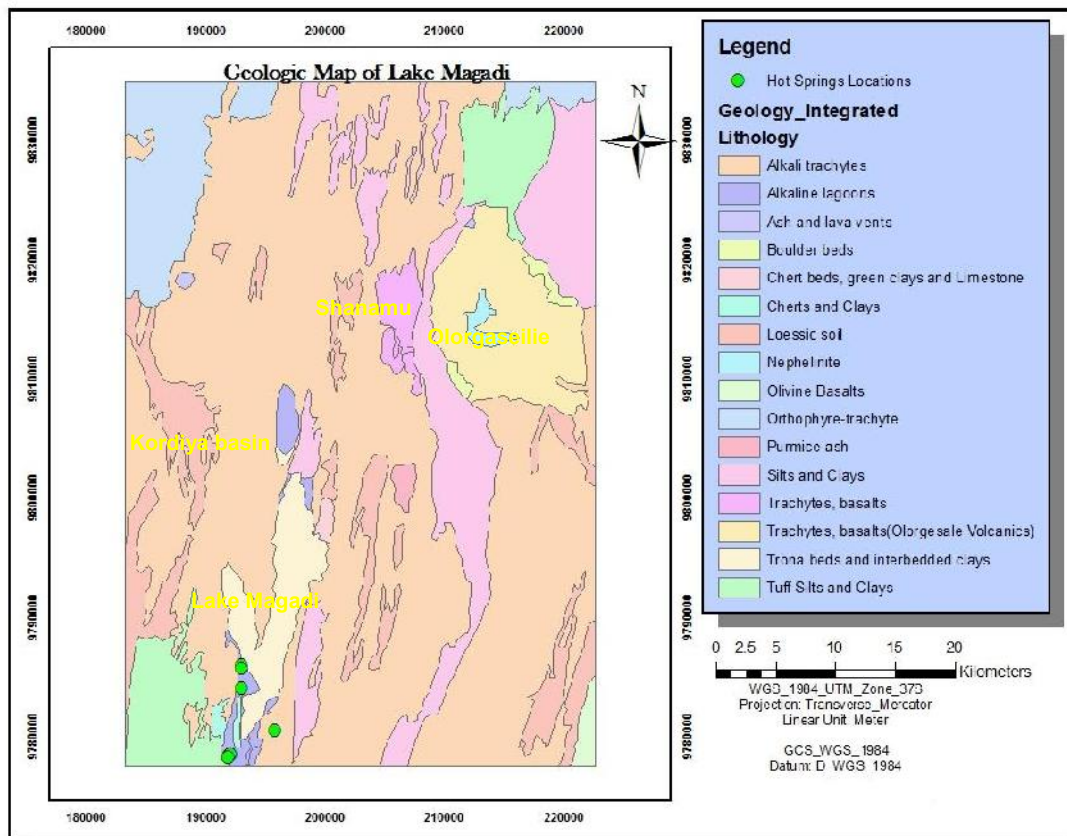164 fault) are revealed at Lake Magadi (Figure 2).
165

192   Figure 3: Simplified Geology map of the study area after [14]

193 **2. METHODOLOGY**
194
195 **2.1. GROUND MAGNETIC DATA**
196
197 Ground and airborne magnetic methods were adopted to study the subsurface geometry of the tectonic
198 faults and their influence of the geothermal resources in Lake Magadi. Since it measures the magnetic
199 field intensity of the Earth, the magnetic technique is capable of mapping subsurface structures such as
200 faults, grabens, horsts and lithology. According to [19], lithology controls magnetic properties through
201 mineralogy, and sharp variation in rock properties generally coincides with lithological contacts.
202 Generally, igneous and metamorphic rocks show significant magnetic properties while sedimentary rocks
203 are mostly non-magnetic [20].

* Tel.: +2348037899856.
E-mail address: aakomolafe@futa.edu.ng
.

204

205 The existence of faults and fractures in the geologic units creates magnetic variations which generate
206 magnetic anomalies. [21] highlight the importance in mapping hydrothermal alteration zones. This is
207 because most magnetic rocks must have been altered and converted from magnetite to pyrite, which in
208 turn results in lower magnetic anomaly than the unaltered zones. In general, the presence of fluid within
209 the faults and fractures would reduce or have no magnetic response. The geometry of subsurface
210 structures can be constructed from magnetic profiles data using various inversion processes. The
211 anomaly due to the near surface and deep source can be enhanced using vertical derivative and upward
212 continuation respectively. Depth to magnetic sources and geometry of the structures can be estimated
213 from Euler's deconvolution method as applied in this study.

214

215 Geometrics 856 Proton Precession Magnetometer was used for the magnetic survey. It is made up of six-
216 digit display of the magnetic field and three digit displays of station, line number and signal strength, and
217 it measures the absolute value of total magnetic field to a resolution of 0.1nT with accuracy of 0.5nT. the
218 equipment is used in various field applications such as geological mapping, mining and location of
219 magnetic materials. Geometrics 856 Proton Precession Magnetometer uses 9 D cell industrial grade
220 batteries and it is connected to magnetic coils mounted on the pole for measurement.

221

222 Five fault systems referred to as A, B, C, D, and E (from west to east) assumed to be the major fluid
223 conduits in the south of the lake, within the basin were identified for ground investigation (Figures 4 and
224 5). Major faults around Lake Magadi are the normal N-S fault, dextral NW-SE fault; strike slip ENE-WSW
225 fault and sinistral NE-SW fault [11, 16]. The N-S faults are well pronounced in the area and are suspected
226 to be the oldest faults in the Lake Magadi area while the youngest are the NE - NW faults. Data were
227 collected perpendicularly to the strike of the four (4) structures in the south of Lake Magadi. Four profiles
228 (P1, P2, P3 and P4) were established to cover a lateral distance of 2.3 km running west–east direction
229 across the hot springs, separated by 330, 330 and 360 meters respectively and located along the lake
230 margins (Figure 5). The profiles cover the area marked by Faults A and D (Figure 4). The latter faults are
231 defined by steep fault scarps. Magnetic measurement was taken at every 25m station along the traverse
232 (west-east direction) with the base station readings taken at every one hour for diurnal correction at the
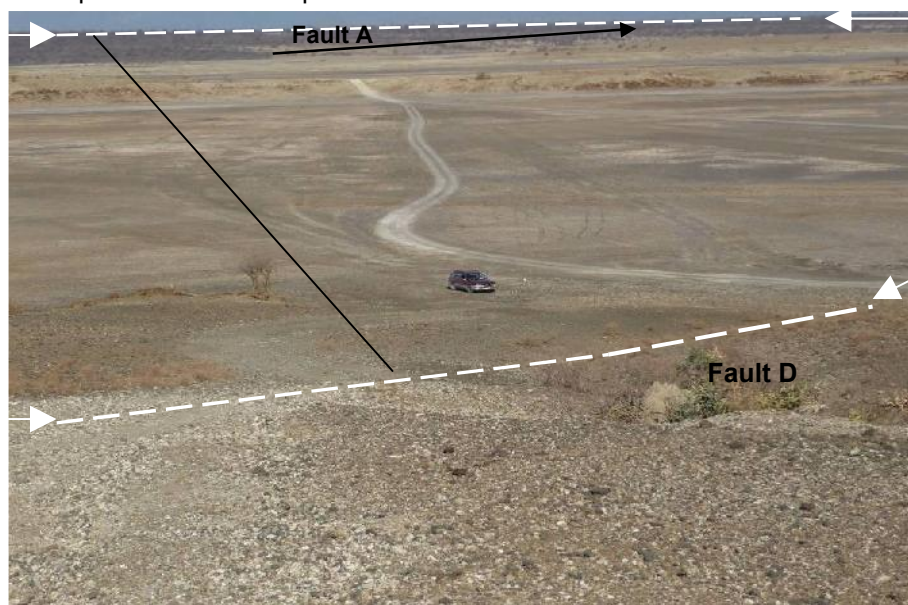233 same position where the previous data was taken.

234
235

236 Figure 4. Field photo showing the magnetic profile extent from Fault A to Fault D (on a west-
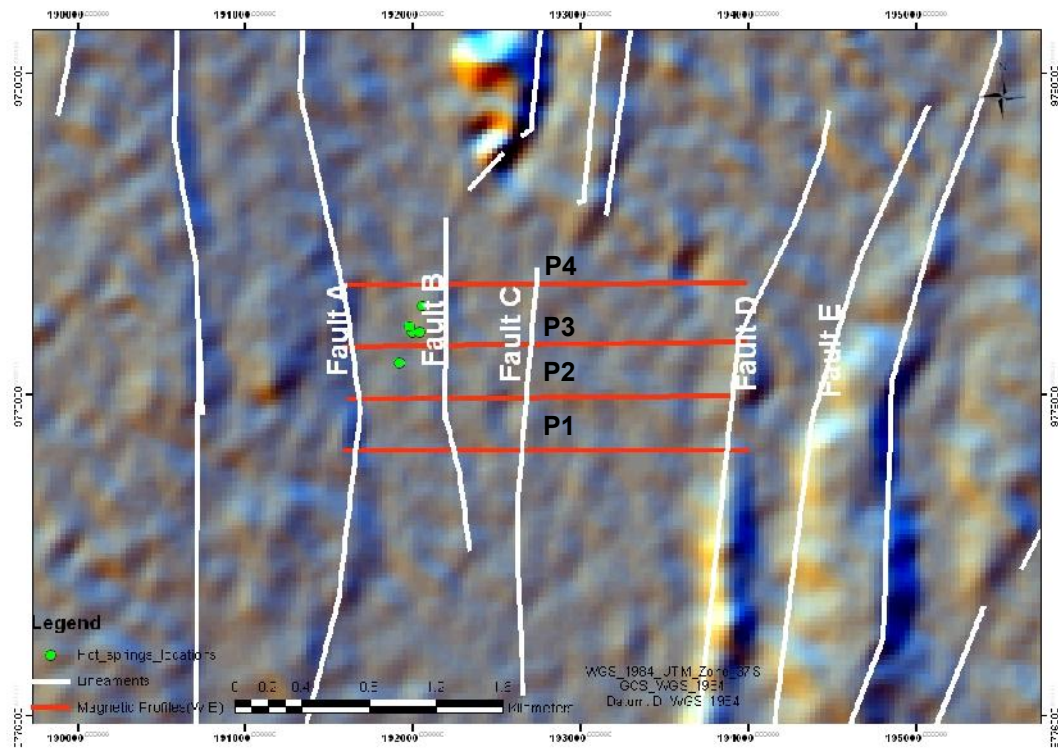237 east direction); the black arrow indicates the North.

238

* Tel.: +2348037899856.
E-mail address: aakomolafe@futa.edu.ng
.

239

240

241

242

243

244

245

246

247
248
249
250
251
252
253
254
255
256
257
258

259
260
261
262
263
264

265

266

Figure 5 **(a)**: Field photo showing the hot springs along the lake margin between Faults A and B. **(b):** Hill-shaded AsterDEM showing the magnetic profiles across the major faults in the study area.

2.2.   DATA PROCESSING

Diurnal Variation Correction

Variation of Earth's magnetic field with time, due to the rotation of the earth and with respect to the solar wind, which may last several hours to one day, is called diurnal variation [22]. In order to correct for drift or diurnal effect in the magnetic readings, a base station within the four magnetic profiles, assumed to be free from magnetic noise was selected. Repeated readings were taken every one hour of the magnetic measurement for the drift correction. Thereafter, the diurnal effect was calculated and the magnetic data

278 were filtered. Noise due to secular change or epoch was considered negligible because consistent
279 measurements were taken at the base station every hour [23].
280
281 **Calculation and Removal of the Geomagnetic Field**
282 Magnetic survey involves measurement of the sum of magnetic field produced by both local and regional
283 magnetic fields. The regional magnetic field, often referred to as geomagnetic field needed to be
284 subtracted from the acquired total magnetic field to obtain the magnetic field anomaly caused by the local
285 source. The geomagnetic field was subsequently calculated using the International Geomagnetic
286 Reference Frame (IGRF) Model 2005 in Geosoft™ Oasis Montaj. This model is calculated based on the
287 dates, elevation and geographical locations (Latitudes and Longitudes) of the observed magnetic data
288 with the generated average geomagnetic field of 33430nT, inclination of -26.2^o and declination of 0.03^o.
289 The IGRF values were subtracted from the observed magnetic values for each station to determine the
290 residual magnetic field due to anomalous contributions from local magnetic sources in the area.
291
292 ## 2.3.   Data Enhancements
293 The corrected magnetic data were presented in grid forms for visualization and further enhancements.
294 The total magnetic intensity (TMI) data were gridded using minimum curvature gridding method with 50m
295 cell size, having the four faults and hot-springs locations overlaid (Figure 6). A minimum curvature surface
296 is the smoothest possible surface that will fit the given data values [24]; It smoothes two straight-line
297 segments by using the Ratio Factor. This gridding method is very effective in the interpolation of gridded
298 points. For effective interpretation of the obtained magnetic data, further enhancements were carried out
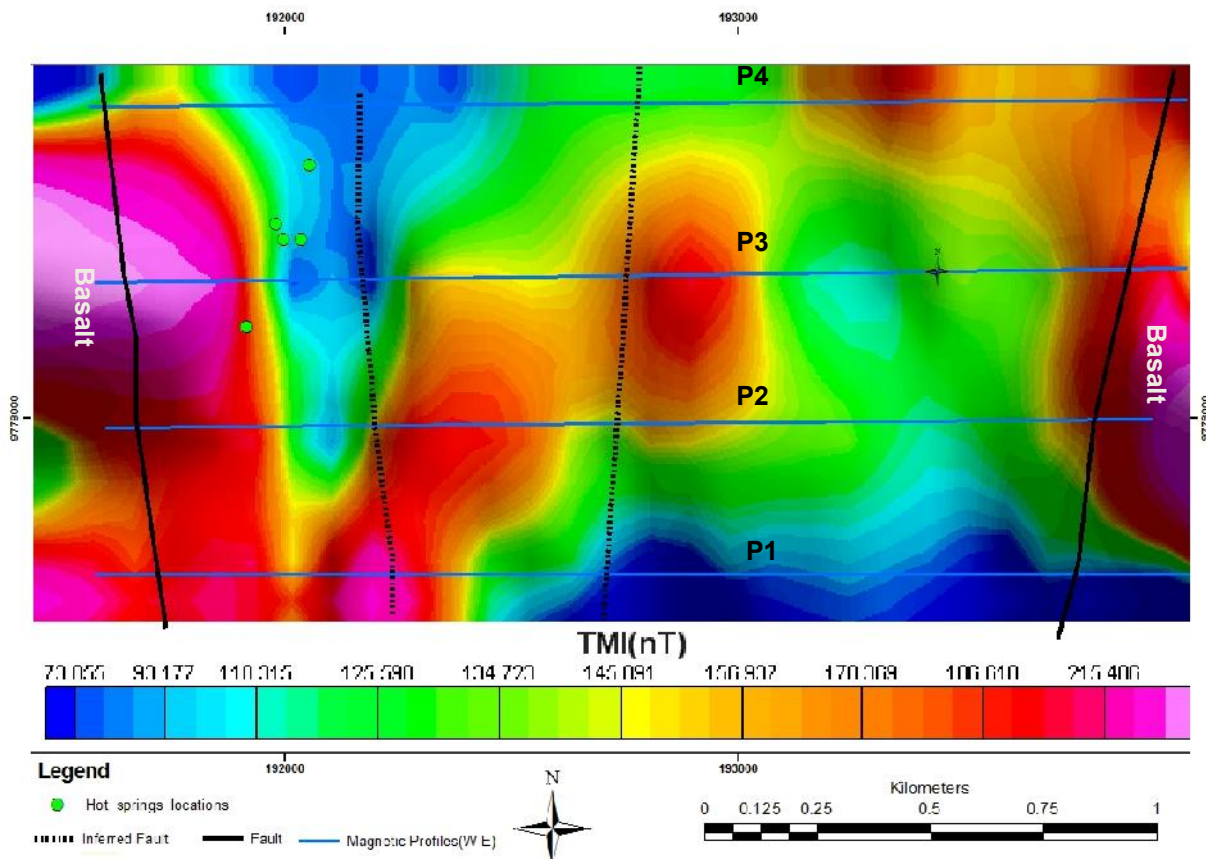299 using various filtering techniques.
300

326 Figure 6: Gridded residual ground Total Magnetic field Intensity (TMI) for the four
327 profiles showing hot springs and faults locations.
328
329

* Tel.: +2348037899856.
E-mail address: aakomolafe@futa.edu.ng
.

Vertical Derivatives

Vertical derivatives of magnetic data generally aid the interpretation process as it enhances and sharpens geophysical anomalies. This filtering method is effective in enhancing anomaly due to shallow sources; it narrows the width of anomalies and very effective in locating source bodies more accurately [25]. Vertical derivative was done by applying low-pass filters to remove high-wavelength, thereby enhancing low-wavelength component of the magnetic spectrum. The vertical derivative of the total magnetic Intensity was derived in Geosoft™ Oasis software as shown in Figure 7.
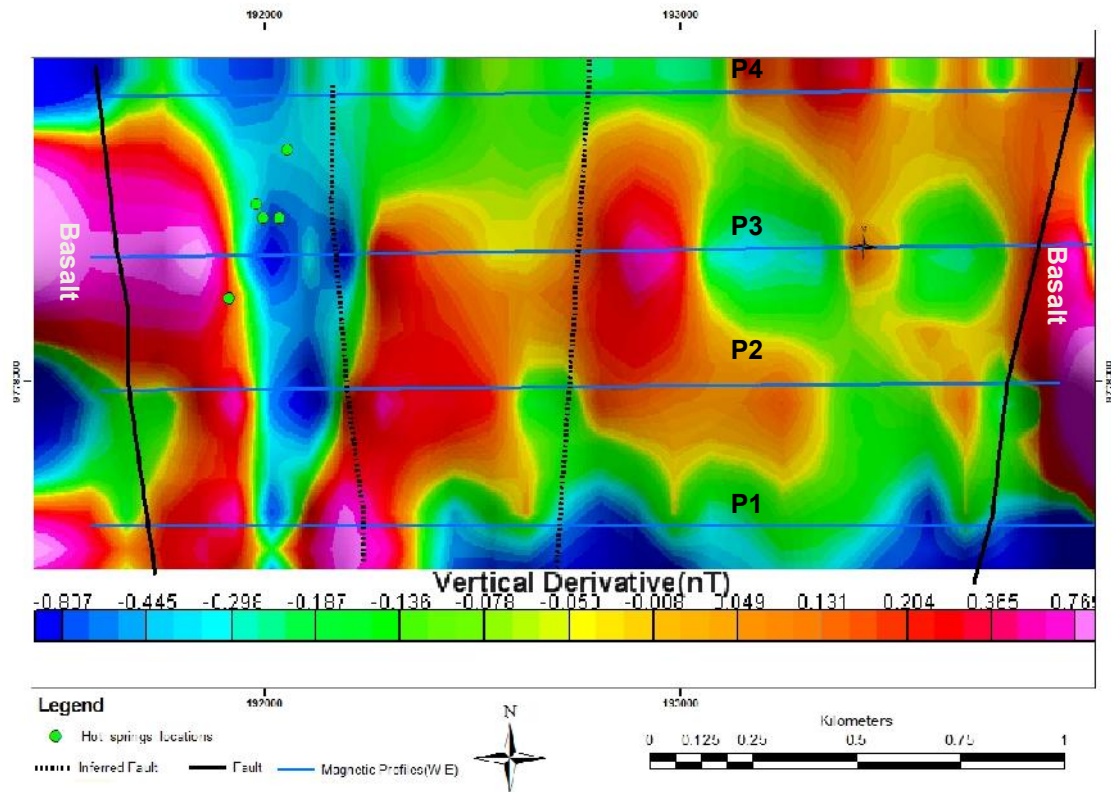

Figure 7: Colour-shaded vertical derivative of the magnetic field intensity showing the shallow magnetic sources.

Analytical Signal

Absolute analytic signal according to [26] can be defined as the square root of the squared sum of the vertical and horizontal derivatives of the magnetic field (Equation 1)

$$AS = \sqrt{\delta x \cdot \delta x + \delta y \cdot \delta y + \delta z \cdot \delta z} \qquad \text{Equation (1)}$$

Where δz is the vertical derivative, δx and δy are the horizontal derivatives and AS is the analytical signal.

The advantage of this method of magnetic data enhancement is that its amplitude function is an absolute value and does not need assumption of the direction of source body magnetization [27]. Analytical signal can be used to locate the edges of remanently magnetized bodies, reveal anomalous textures and highlight discontinuities [28]. The analytical signal derived from the obtained magnetic data enhances the edges of the major structures in the study area (Figure 8).

* Tel.: +2348037899856.
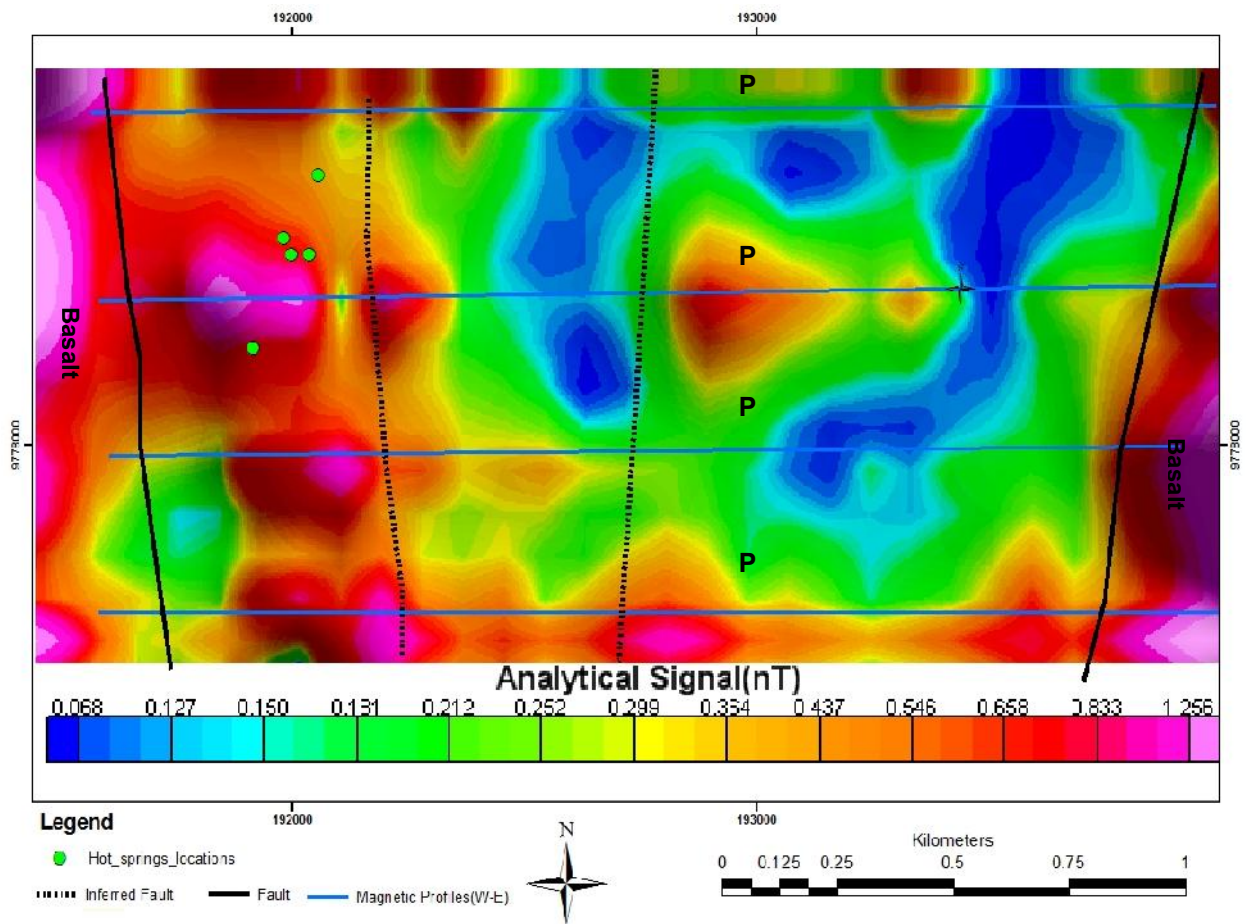E-mail address: aakomolafe@futa.edu.ng

.

Figure 8: Colour -shaded Analytical signal maps of the four profiles

Euler Deconvolution

Euler deconvolution is an inversion method for estimating location and depth to magnetic anomaly source. It relates the magnetic field and its gradient components to the location of the anomaly source with the degree of homogeneity expressed as a structural index and it is the best suited method for anomalies caused by isolated and multiple sources [29]. The structural index (SI) is a measure of the fall-off off the field with distance from the source. Euler deconvolution is expressed in Equation (2) as:

$$(x - x_o)\delta T / \delta x + (y - y_o)\delta T / \delta y + (z - z_0)\delta T / \delta z = N(B - T) \qquad \text{Equation (2)}$$

where (x_o, y_o, z) is the source position of a magnetic source whose total field T is measured at x, y, z, while B is the regional value of the total field, and N is expressed as the structural index (SI), a measure of the rate of change with distance of the potential field, depending on the geometry of the source [29].

Estimating depth to magnetic anomaly using Euler deconvolution involves the following: i) Reduction to the pole; ii) Calculation of horizontal and vertical gradients of magnetic field data, calculated in frequency domain; iii) choosing window sizes; and iv) structural index, e.g. contact, dike and point [29]. In general, the desired structural indices are chosen with the window size for depth determination. This is set based on the anomaly of interest. In this study, both 3D and 2D Euler deconvolution were adopted for both the gridded and profile data respectively.

2D Euler Deconvolution

Two- dimensional Euler deconvolution was generated from the software developed by [30] for constraining the subsurface geometry along the profile lines. The software requires magnetic parameters such as the geomagnetic field, survey locations, inclinations and declination angles. Two columns with a

* Tel.: +2348037899856.
E-mail address: aakomolafe@futa.edu.ng

.

438 space delimited ASCII file are required for input; the first column is the magnetic station locations while
439 the second column is the corrected magnetic field values. The results of the IGRF was used as the inputs
440 for this process, i.e. geomagnetic field intensity of 33430nT, inclination of -26.2^o and declination of 0.03^o.
441 Similar to the 3D Euler deconvolution, the structural indices and the Euler window size must be selected.
442 In this research, a window size of 13, 110m X-separation and 55m Y separation were adopted. To better
443 constrain the subsurface geology, 1.0 structural index (steep contact) which is an indication of faults
444 contacts were plotted for all the traverses; these are shown in Figures 11- 14 respectively.
445
446 **3D Euler Deconvolution**
447 3D Euler deconvolution was performed on the total magnetic intensity (TMI) grid data using standard
448 Euler deconvolution. This was done to locate depths to the lithology contacts on the gridded map. The
449 best clustering Euler depths was achieved using solution window size of 4, 1.0 structural index (SI) (steep
450 contact) and 15% depth tolerance. The results were plotted on the analytical signal map for effective
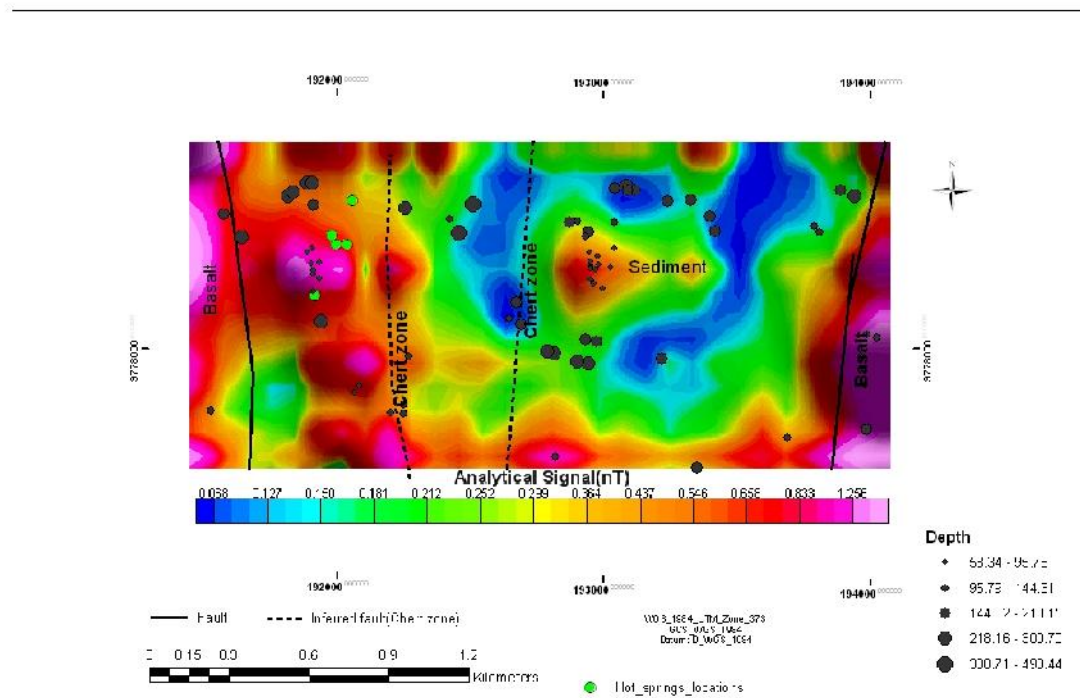451 interpretations (Figure 9).
452
453

454
455 Figure 9: 3D Euler's depths solutions (structural index of 1) plotted on the colour shaded
456 analytical signal map.

457

458 **2.4.   Aeromagnetic Data**
459 The aeromagnetic data used in this study was part of the African Magnetic Mapping Project (AMMP),
460 which was intended to compile airborne magnetic data for some parts of Africa. Aeromagnetic data in the
461 study area was acquired by the Compagnie Generale de Geophysique (CGG) in 1987 with 2km line
462 spacing, flight direction of 90° (W-E) and flying height of 2896m above sea level.
463
464 Magnetic data on flight lines 320 and 322, covering about 7.7 km long from the total magnetic intensity
465 map of the aeromagnetic data are shown in Figure 10. The data processing (levelling correction and
466 geomagnetic field removal) was done by AMMP. The magnetic grid was created using 1km cell size with

* Tel.: +2348037899856.
E-mail address: aakomolafe@futa.edu.ng
.

467 AMMP grid projection system, re-projected to WGS84, UTM 37S projection later to conform to the
468 projection used in this study. Lake Magadi study area was clipped from the entire gridded data as shown
469 in Figure 10. The extracted aeromagnetic data were processed and inverted using 2D Euler
470 deconvolution software developed by [30] and following the same procedures and processing adopted in
471 the ground magnetic method. In this case, the results from IGRF 2005 model calculated from the
472 magnetic data were the magnetic intensity of 33414, inclination of -26.3^0 and declination of 0.002^0 with
473 structural index of 1 (steep contacts). These were used as inputs to the Euler's software to construct the
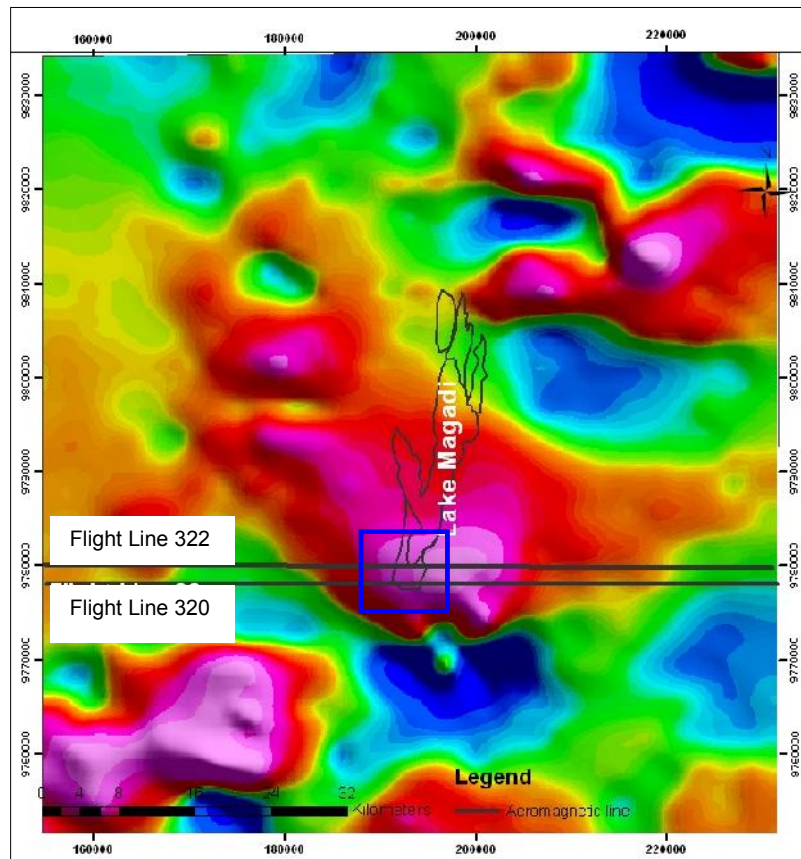474 subsurface magnetic sources along the selected profile lines (Figures 16 and 17).

475

476
477 Figure 10: Colour-shaded Aeromagnetic Total Magnetic Intensity (TMI) grid
478 data for Lake Magadi area, showing the extracted lines 322 and 320.

479

3. DATA INTERPRETATION

481 From the Total Magnetic Intensity (TMI) grid data, the high intensity magnetic signals at the western
482 margins mark the faults with basaltic rocks (Figure 6) while the eastern margin shows a decay of the
483 magnetic intensity corresponding to the end of the basalts and marking the onset of the chert zone. The
484 basin is characterized by low magnetic signatures, which can be attributed to the presence of fluids. The
485 two-chert zones show reasonably high magnetic anomaly in the TMI grid (Figure 6). In the vertical
486 derivative map (Figure 7), the hot springs, which are clearly manifested in the surface between the north-
487 south trending Fault A, and Fault B in the south west show low (negative) magnetic anomaly. The map
488 also shows the lateral continuity N-S faults along the axial rift zone. High magnetic signal within the basin
489 coincides with the Fault zones (B and C) (Figures 6 and 7). The analytic signal map (Figure 8) shows that
490 the survey area is inside a basin surrounded by the west, east Faults A and D. In this map, the edges of
491 the magnetic anomaly are better enhanced and it clearly shows the zones of discontinuities between
492 each geologic unit, especially the major faults in the area. Majority of the hot springs occurs within a

* Tel.: +2348037899856.
E-mail address: aakomolafe@futa.edu.ng
.

boundary between high and moderate magnetic intensity rocks. The location of hot spring is characterized by very low and negative anomaly as revealed in the vertical derivative map (Figure 7). The sediments further bury the basaltic rocks outcropping at the hot springs south; these are probably responsible for the high magnetic anomaly, which are evident in the analytical signal map (Figure 8). Within the basin is a localized high magnetic anomaly, which can be attributed to the presence of volcanic rocks. From the depth estimation, the basin depth between 300 and 493 metres, with the western and eastern basalts from the Euler's depth extending to about 300m.

3.1. 2D INTERPRETATION OF THE MAGNETIC DATA ALONG THE TRAVERSES

Qualitative interpretation of the magnetic traverses shows that the basin is bounded by N-S trending faults both to the west and to the east. The 2D magnetic profiles (Figures 11 – 14) show the magnetic anomaly observed over the four faults in the south of Lake Magadi. The differences in magnetic anomaly signatures possibly indicate structurally controlled subsurface features [23, 31].
Figure 11(b) shows magnetic anomaly along traverse P1. Here, four distinct trends are recognized, which coincide with the location of the identified faults within the basin. The traverse begins with a high and low magnetic anomaly (Station 0 – 200m), which is attributed to the highly faulted basaltic dyke that bounds the basin to the west (Figure 11 a and b). This signature is followed to the east by generally low signatures (Station 200 – 380m). This very low magnetic anomaly coincides with the hot and cold spring locations within the basin. The same result was experienced in Ethiopian Rift Valley by Abiye and Tigistu [21]. The lack of magnetic sources exists mostly between the faults, an evident of the presence of fluids as experienced in the field. The discontinuity between the basalt and sediments basin show the existence of faults between the rock units. A gentle rise in the anomaly towards the east (Station 380 -500m) shows the commencement of the chert zone within Fault B followed by low signatures characterized by sediments (Station 500 -700m). The high magnetic response within this zone could be attributed to the presence of chert vein as observed in the field. At the end of the low anomaly, there is a little rise but undulating signatures (Station 700m) which commence the chert zone (Fault C), followed by a relatively low anomaly (up to Station 1700m). The eastern-most basaltic rock along the traverse shows a rise in magnetic anomaly. General fluctuation of the magnetic response along the profile and the scattering of the Euler solutions possibly indicate that series of intense tectonic/faulting activity associated with shearing might have taken place within the basin [23, 31].

* Tel.: +2348037899856.
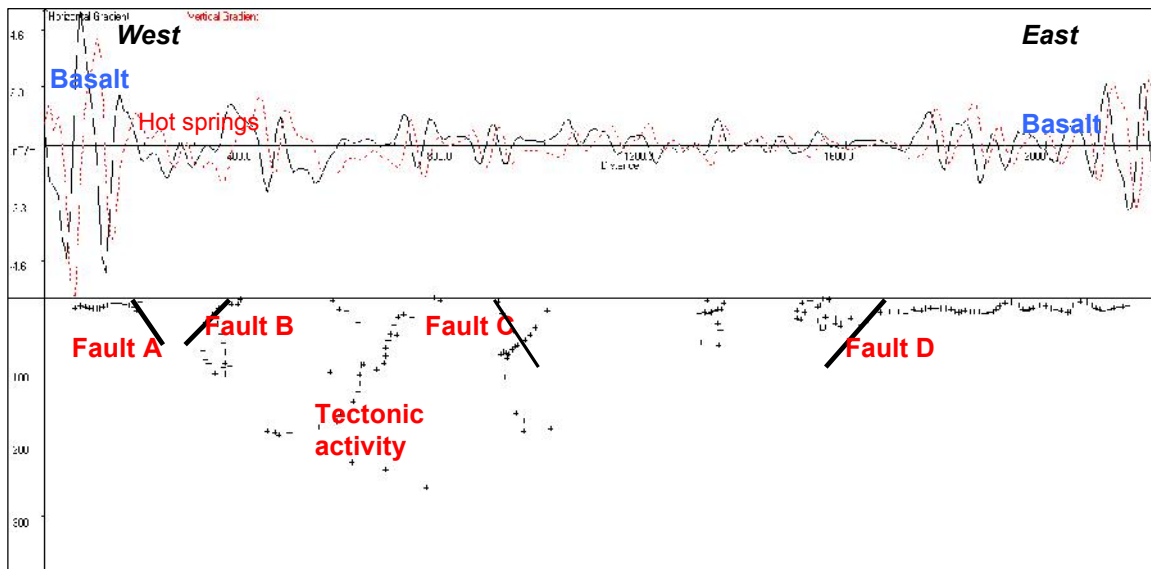E-mail address: aakomolafe@futa.edu.ng

.
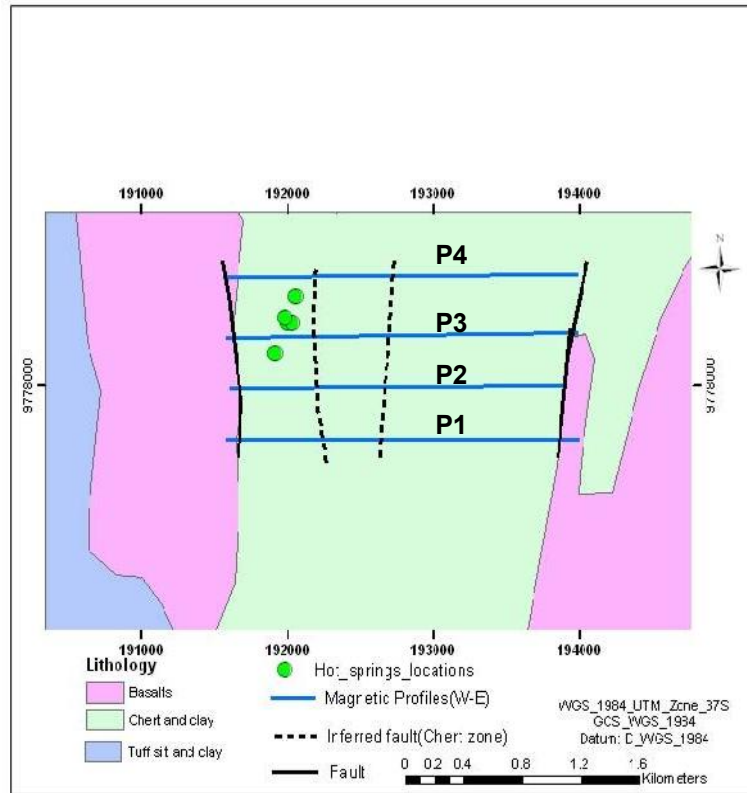
Figure 11 **a** Geologic map of the magnetic survey area. **(b)**. Processed ground magnetic data with 2 D Euler solutions obtained along traverse one with inclination and declination angles of -26.2^o and 0.03^o respectively. Plus (+) signs are Euler solutions for 1.0 structural index.

Traverses P2 and P3 (Figures 12 and 13) shows similar variation in magnetic signatures as traverse P1. Traverse P3 has well-defined faults, corresponding to Faults B, C, and D. The variation in magnetic amplitudes and the much scattering in the Euler solution could be attributed to an intense shearing activity and localized anomaly beneath the profiles, which is also visible in the analytical map. These scatterings are not seen in the fourth profile (Figure 14). Profile Four (P4) shows consistent high and low

* Tel.: +2348037899856.
E-mail address: aakomolafe@futa.edu.ng
.

magnetic responses along the transverse. These undulating signatures and the Euler deconvolution solutions clearly show the subsurface faulting/contact pattern within the geological units. The subsurface fault geometry as revealed in Traverse Four shows a general normal faulting system associated with Magadi N-S faults. Generally in all the traverses, Faults A and D show both eastern and western dip respectively. These faults are major structures bounding the basin in the southern part of Lake Magadi.
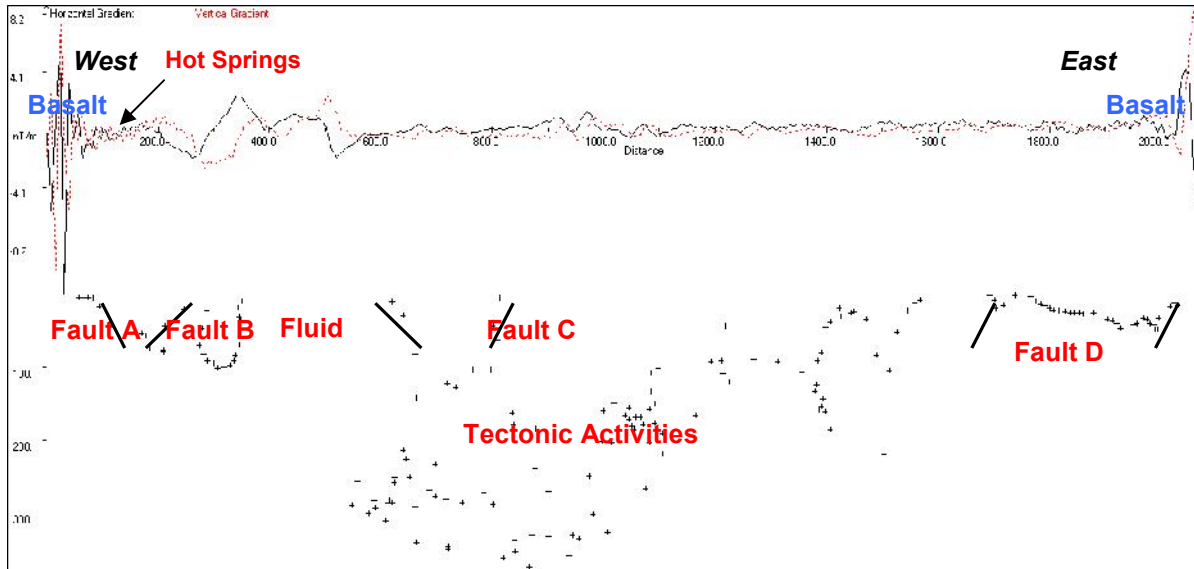

Figure 12. Processed ground magnetic data with 2D Euler solutions obtained along Traverse Two with inclination and declination angles of -26.2^o and 0.03^o respectively. Plus (+) signs are Euler solutions for 1.0 structural index.
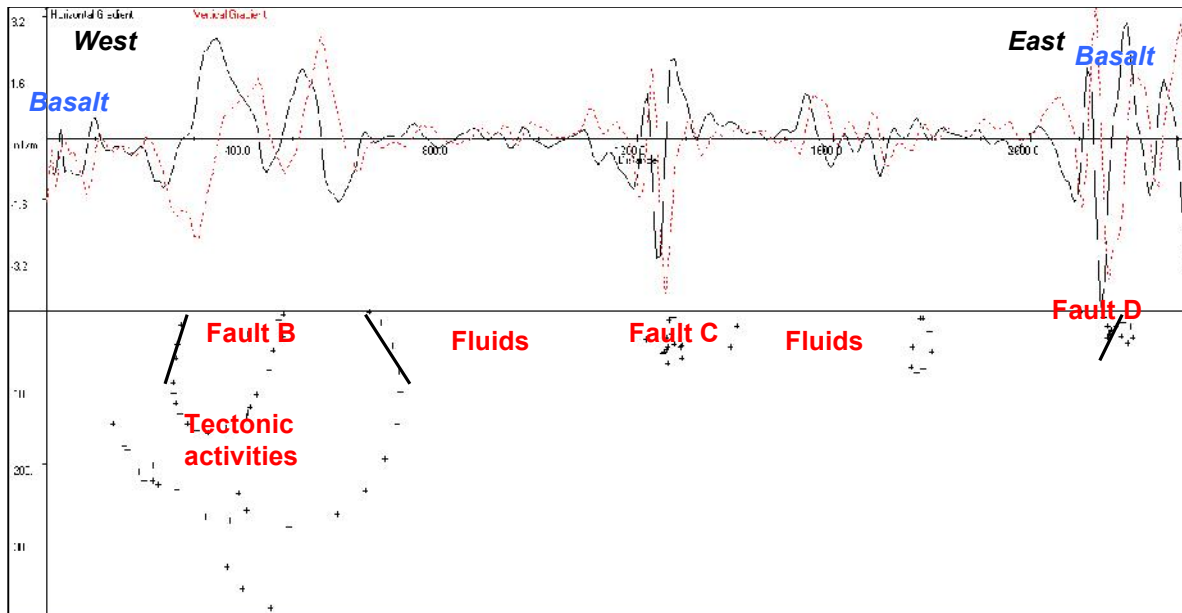

Figure13. Processed ground magnetic data with 2D Euler solutions obtained along Traverse Three with inclination and declination angles of -26.2^o and 0.03^o respectively. Plus (+) signs are Euler solutions for 1.0 structural index.

* Tel.: +2348037899856.
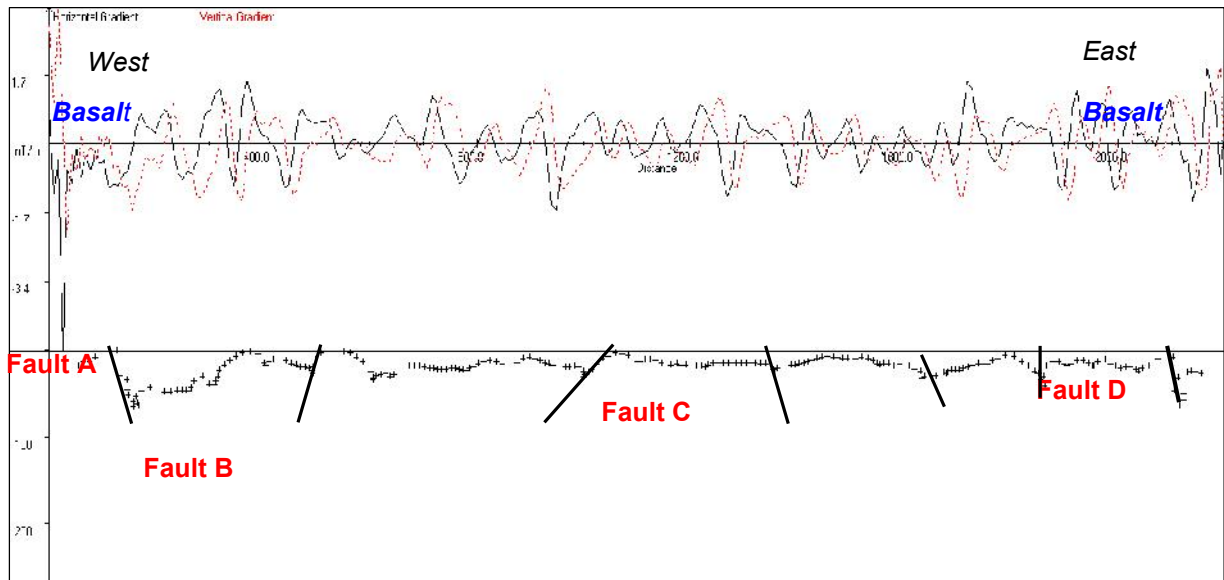E-mail address: aakomolafe@futa.edu.ng

.

549

550 Figure 14. Processed ground magnetic data with 2D Euler solutions obtained along Traverse Four

551 with inclination and declination angles of -26.2^{o} and 0.03^{o} respectively. Plus (+) signs are Euler

552 Evidently, the results of the magnetic profiles confirmed the investigation done by [8] using electrical
553 resistivity method (Figure 15). Their resistivity profiles showed the tectonic activities up to the depth of
554 75m with well-defined geological units comprising faults splay both to west and east. The faults, which are
555 normal trending N-S are parallel faults that bounds Lake Magadi graben east and west, and they play
556 prominent role in the transportation of the geothermal fluid from the subsurface to the surface. The
557 scattering euler deconvolution in magnetic profiles confirmed the fracture zone delineated from the
558 geoelectric profiles as reported by Komolafe et al. [8]. The faults (A, B, C, and D) were further probed to a
559 deeper depth using airborne magnetic data as discussed in the next section.
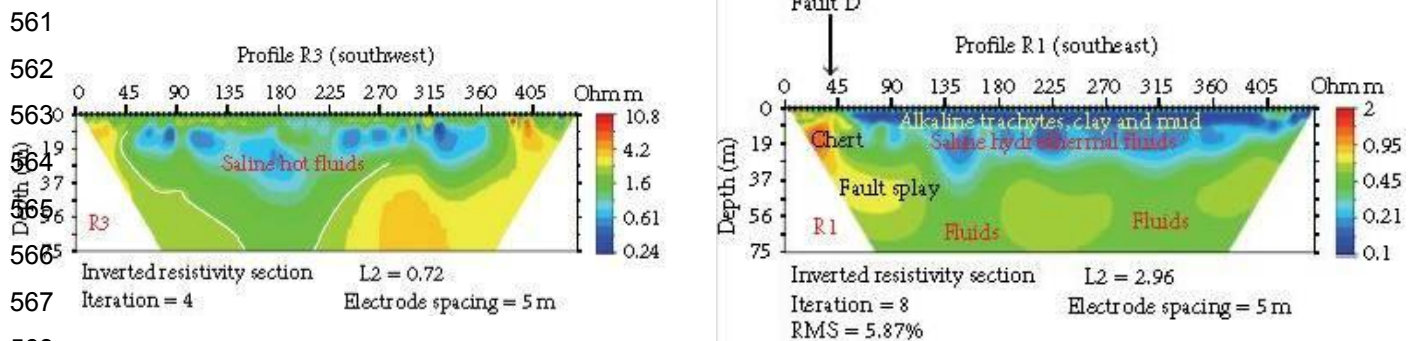
560

561

562

568

569 Figure 15 (a) Inverted 2D resistivity section for profile 3 between fault A and fault B in the southwest of
570 Lake Magadi (b) Inverted 2D resistivity section for profile 1 across fault D and towards fault E in the
571 southeast of Lake Magadi after Komolafe et al. [8].

572

573 ## 3.2.   2D INTERPRETATION OF THE AEROMAGNETIC PROFILES

574 The processed aeromagnetic data for lines 320 and 322 are shown in Figures 16 and 17. The flight lines,
575 which are 2km, separated from each other shows similar subsurface geometry, both in frequency and
576 amplitudes. Most of the Euler solutions are concentrated along the rift axis while the basin is marked by
577 the absence of magnetic sources. These observations are in line with the results experienced in the
578 northern part of the Kenya rift by [32]. The magnetic sources from 2D Euler correspond approximately to
579 the top of the magnetic sources. These sources reflect rock beneath the thick sediment within the axial

* Tel.: +2348037899856.
E-mail address: aakomolafe@futa.edu.ng
.

580 part of the rift basin/trough. The sub-vertical alignment and scattering of the Euler solutions reveals the
581 existence of tectonic activities [23, 33-34] which extends to a depth of 7.5 km (Figures 16b and 17b). The
582 magnetic sources correspond largely to the tectonic structures (faults). These tectonic structures,
583 approximately at a depth of 7.5km, correspond to the established surface N-S faults A, D and E in the
584 south of Lake Magadi, which bounds the basin in the surface as seen in the topographic profiles (Figure
585 16a and 17b). The lack of magnetic signal between the faults in the subsurface could be because of the
586 presence of hydrothermal fluids within the basin. Faults B and C are mostly shallow; they are not clearly
587 manifested in the aeromagnetic profiles, but are visible in the ground magnetic profiles.
588
589

590
591 Figure 16. **(a)** Extracted topography elevations of Lake Magadi area from Aster DEM along flight line
592 330 showing surface faults and grabens. **(b)** 2D Euler deconvolution solutions from aeromagnetic data
593 along flight line 320. The plus (+) signs are structural index of 1 with inclination and declinations of -26.3[0]
594 and 0.002[0] respectively.
595
596
597
598
599

* Tel.: +2348037899856.
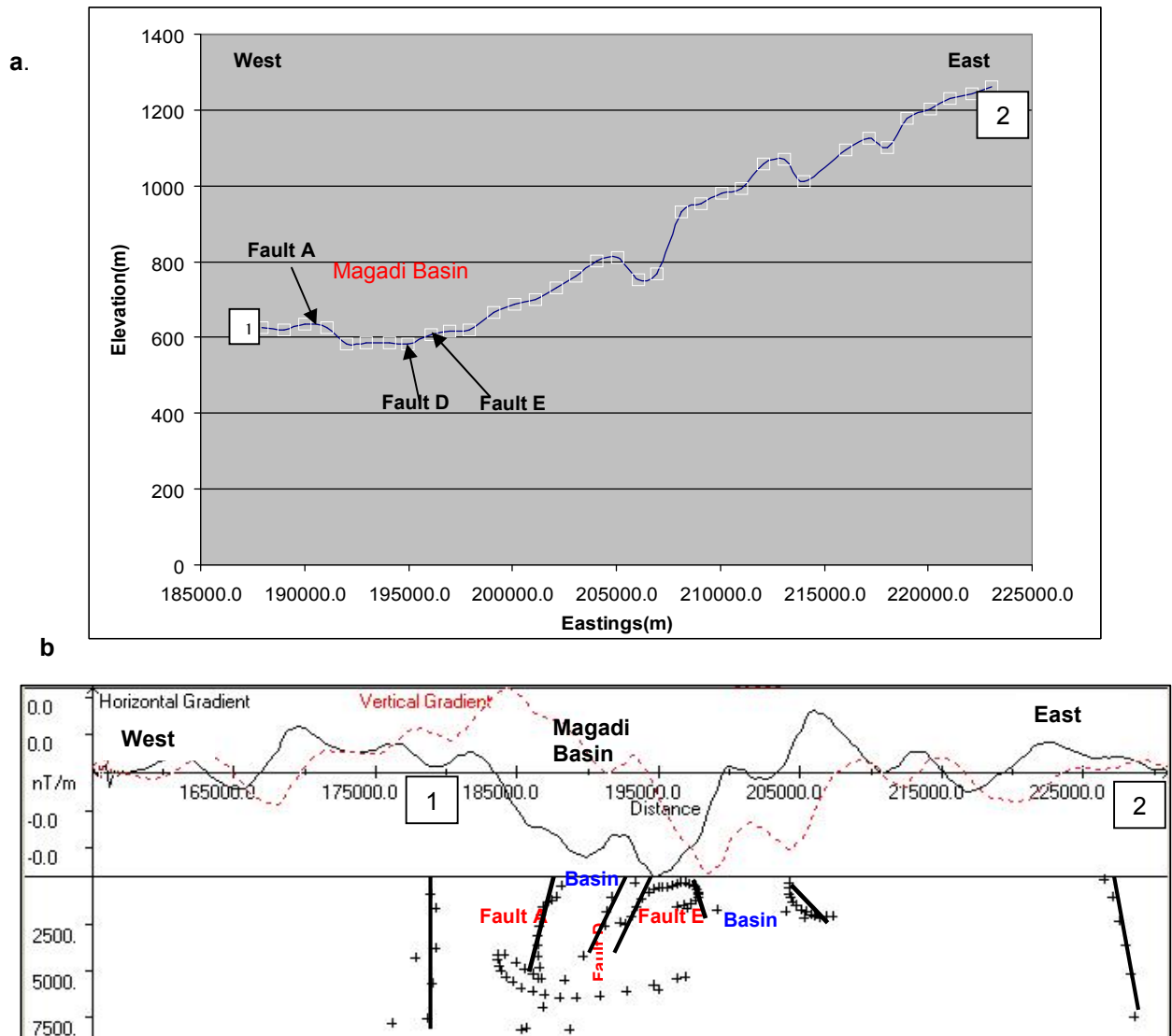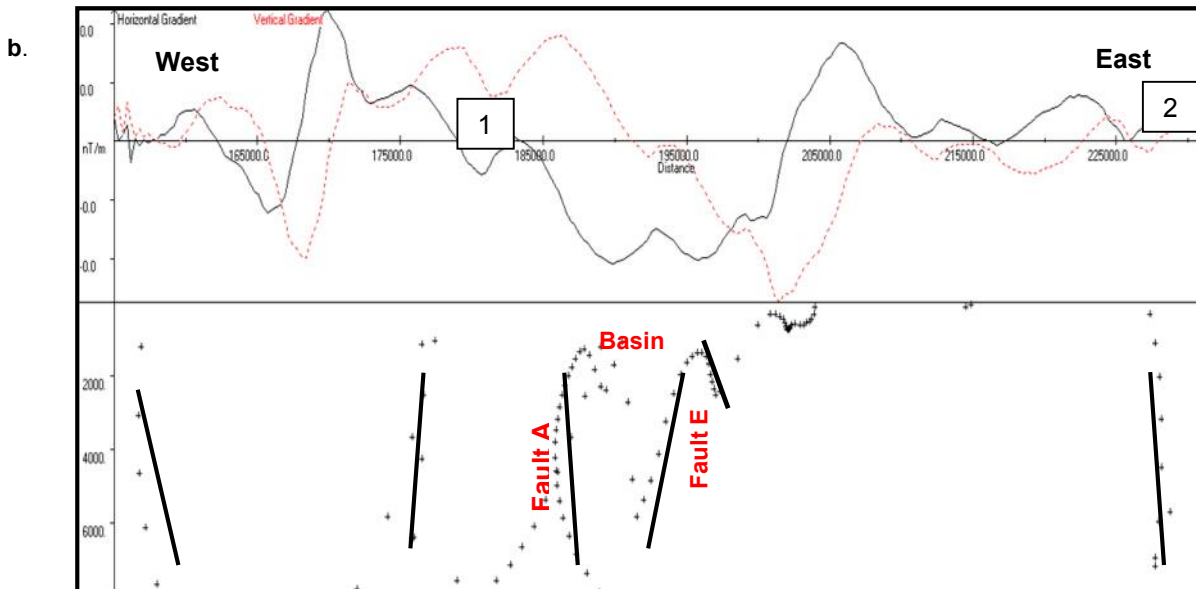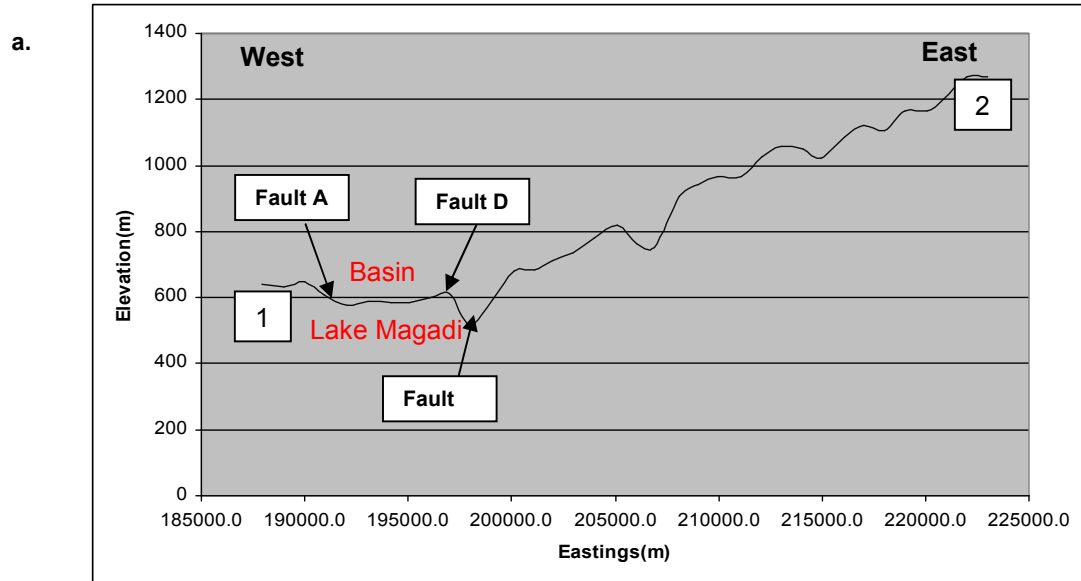E-mail address: aakomolafe@futa.edu.ng
.

Figure 17 .(a) Extracted topography elevations of Lake Magadi area from Aster DEM along flight line 322 showing surface faults and grabens. (b) 2D Euler deconvolution solutions from aeromagnetic data along flight line 322. The plus signs are structural index of 1

CONCLUSIONS

Detailed analysis of ground and aeromagnetic data has revealed that the Lake Magadi area is highly faulted. The multiple scattering of Euler solution in the ground magnetic profiles confirms this highly fractured and faulted zone within the subsurface. The location of the fluid filled zone within the basin is marked by the absence of magnetic source in the grids and 2D Euler's deconvolution solutions of the ground magnetic data. These fluid zones exist between the investigated tectonic lineaments as confirmed by Komolafe [8].

This tectonic activity in the Lake Magadi upper crust contributes to the upward flow of hydrothermal fluids from the hot geothermal reservoir to the surface. It was established that the surface lineaments and

* Tel.: +2348037899856.
E-mail address: aakomolafe@futa.edu.ng
.

tectonic activities along and beneath Magadi Basin extends deeply to the subsurface (approximately 7.5km), with surface expressions showing as faults which bind the graben to the west and to the east. It was observed that the existence of the structures south of Lake Magadi plays an important role in creating a flow path through which the hydrothermal fluids (hot or cold) are transported to the surface. Therefore, the manifestations of hot springs and trona deposit in the south of Lake Magadi are largely supported by the presence of N-S faults in the area.

ACKNOWLEDGEMENT

REFERENCES

1. Simiyu, S.M. and G.R. Keller, Seismic monitoring of the Olkaria Geothermal area, Kenya Rift valley. Journal of Volcanology and Geothermal Research, 2000. **95**(1-4): p. 197-208.
2. Gudmundsson, A., et al., Fracture networks and fluid transport in active fault zones. Journal of Structural Geology, 2001. **23**(2-3): p. 343-353.
3. Lerner, E.K.L. and B.W.L.G. Cengage. Faults and Fractures. 2003; Available from: http://www.enotes.com/earth-science.
4. Mary, H.D. and F. Mario, What is Geothermal Energy? 2004, Istituto di Geoscienze e Georisorse: Pisa, Italy. p. 1-61.
5. Mwaura, F., A spatio-chemical survey of hydrogeothermal springs in Lake Elementaita, Kenya. International Journal of Salt Lake Research, 1999. **8**(2): p. 127-138.
6. Jones, B.F., H.P. Eugster, and S.L. Rettig, Hydrochemistry of the Lake Magadi basin, Kenya. Geochimica et Cosmochimica Acta, 1977. **41**(1): p. 53-72.
7. Maguire, P.K.H. and R.E. Long, The Structure on the Western Flank of the Gregory Rift (Kenya). Part I. The Crust. Geophysical Journal of the Royal Astronomical Society, 1976. **44**(3): p. 661-675.
8. Komolafe, A.A., et al., Integrated Remote Sensing and Geophysical Investigations of the Geodynamic Activities at Lake Magadi, Southern Kenyan Rift. International Journal of Geophysics, 2012. **2012**: p. 15.
9. Stampolidis, A. and G.N. Tsokas, Curie Point Depths of Macedonia and Thrace, N. Greece. Pure and Applied Geophysics, 2002. **159**(11): p. 2659-2671.
10. Spector, A. and F.S. Grant, Statistical models for interpreting aeromagnetic data. Geophysics 1970. **35**: p. 293–302.
11. Atmaoui, N. and D. Hollnack, Neotectonics and extension direction of the Southern Kenya Rift, Lake Magadi area. Tectonophysics, 2003. **364**(1-2): p. 71-83.
12. Eugster, H.P., Chemistry and origin of brines of Lake Magadi, Kenya. Mineral. Soc. Amer. Spec. Paper, 1970. **No. 3**: p. 215 - 235.
13. Smith, M. and P. Mosley, Crustal Heterogeneity and Basement Influence on the Development of the Kenya Rift, East Africa. Tectonics, 1993. **12**.
14. Baker, B.H., Geology of the Magadi area. 1958, Geological Survey of Kenya, Nairobi.
15. Baker, B.H., et al., Sequence and geochronology of the Kenya rift volcanics. Tectonophysics, 1971. **11**(3): p. 191-215.
16. Sequar, G.W., Neotectonics of the East African rift system : new interpretations from conjunctive analysis of field and remotely sensed datasets in the lake Magadi area, Kenya. 2009, ITC: Enschede. p. 99.
17. Simiyu, S.M. and G.R. Keller, Upper crustal structure in the vicinity of Lake Magadi in the Kenya Rift Valley region. Journal of African Earth Sciences, 1998. **27**(3-4): p. 359-371.
18. Le Turdu, C., et al., Influence of pre-existing oblique discontinuities on the geometry and evolution of extensional fault patterns; Evidence from the Kenya Rift using Spot Imagery. In: C.K. Morley (Editor), Geoscience of Rift systems-Evolution of East Africa. AAPG studies in Geology, 1999: p. 173-191.

* Tel.: +2348037899856.
E-mail address: aakomolafe@futa.edu.ng
.

671   19.   Jessell, M., Three-dimensional geological modelling of potential-field data. Computers &
672   Geosciences, 2001. **27**(4): p. 455-465.
673   20.   Clark, D.A. and D.W. Emerson, Notes on rock magnetization characteristics in applied
674   geophysical studies. Exploration Geophysics, 1991. **22**(3): p. 547-555.
675   21.   Abiye, T.A. and H. Tigistu, Geophysical exploration of the Boku geothermal area, Central
676   Ethiopian Rift. Geothermics, 2008. **37**(6): p. 586-596.
677   22.   Riddihough, R.P., Diurnal Corrections To Magnetic Surveys—An Assessment Of Errors.
678   Geophysical Prospecting, 1971. **19**(4): p. 551-567.
679   23.   Adepelumi, A.A., et al., Integrated geophysical mapping of the Ifewara transcurrent fault system,
680   Nigeria. Journal of African Earth Sciences, 2008. **52**(4-5): p. 161-166.
681   24.   Briggs, I.C., Machine Contouring Using Minimum Curvature. GEOPHYSICS, 1974. **39**(1): p. 39-
682   48.
683   25.   Cooper, G.R.J. and D.R. Cowan, Filtering using variable order vertical derivatives. Computers &
684   Geosciences, 2004. **30**(5): p. 455-459.
685   26.   Roest, W.R., J. Verhoef, and M. Pilkington, Magnetic interpretation using the 3-D analytic signal.
686   Geophysics 1992. **57**: p. 116–125.
687   27.   Jeng, Y., et al., Integrated signal enhancements in magnetic investigation in archaeology. Journal
688   of Applied Geophysics, 2003. **53**(1): p. 31-48.
689   28.   MacLeod, I.N., K. Jones, and T.F. Dai, 3-D analytic signal in the interpretation of total magnetic
690   field data at low magnetic latitudes. Exploration Geophysics, 1993. **24**(4): p. 679-688.
691   29.   El Dawi, M.G., et al., Depth estimation of 2-D magnetic anomalous sources by using Euler
692   deconvolution method. American Journal of Applied Sciences 2004.
693   30.   Cooper, G.R.J., Euler deconvolution applied to potential field gradients. Exploration Geophysics,
694   2004. **35**(3): p. 165-170.
695   31.   Telford, W.M., L.P. Geldart, and R.E. Sheriff, Applied Geophysics. second ed. Vol. 1. 1976:
696   Cambridge University Press. 50-102.
697   32.   Mariita, N.O. and G.R. Keller, An integrated geophysical study of the northern Kenya rift. Journal
698   of African Earth Sciences, 2007. **48**(2-3): p. 80-94.
699   33.   Mushayandebvu, M.F., et al., Magnetic source parameters of two-dimensional structures using
700   extended Euler deconvolution. Geophysics, 2001. **66**(3): p. 814-823.
701   34.   Kuria, Z.N., et al., Active fault segments as potential earthquake sources: Inferences from
702   integrated geophysical mapping of the Magadi fault system, southern Kenya Rift. Journal of
703   African Earth Sciences, 2010. **57**(4): p. 345–359.
704
705

* Tel.: +2348037899856.
E-mail address: aakomolafe@futa.edu.ng

.